# Measurement of the $n-p$ Elastic Scattering Angular Distribution at $E_n = 14.9$ MeV

N. Boukharouba,[1] F.B. Bateman,[2] A.D. Carlson,[2] C.E. Brient,[3]
S.M. Grimes,[3] T.N. Massey,[3] R.C. Haight,[4] and D.E. Carter[5]

[1] *Department of Physics, University of Guelma, Guelma 24000, Algeria*
[2] *National Institute of Standards and Technology, Gaithersburg, MD 20899*
[3] *Department of Physics and Astronomy, Ohio University, Athens, OH 45701, USA*
[4] *Los Alamos Neutron Science Center, Los Alamos National Laboratory, Los Alamos, NM 87545, USA*
[5] *Institute of Nuclear and Particle Physics, Ohio University, Athens, OH 45701, USA*

The relative differential cross section for the elastic scattering of neutrons by protons was measured at an incident neutron energy $E_n = 14.9$ MeV and for center-of-mass scattering angles ranging from about 60° to 180°. Angular distribution values were obtained from the normalization of the integrated data to the $n-p$ total elastic scattering cross section. Comparisons of the normalized data to the predictions of the Arndt et al. phase-shift analysis, those of the Nijmegen group, and with the ENDF/B-VII.0 evaluation, are sensitive to the value of the total elastic scattering cross section used to normalize the data. The results of a fit to a first order Legendre polynomial expansion are in good agreement in the backward scattering hemisphere with the predictions of the Arndt et al. phase-shift analysis, those of the Nijmegen group and, to a lesser extent, with the ENDF/B-VII.0 evaluation. A fit to a second order expansion is in better agreement with the ENDF/B-VII.0 evaluation than with the other predictions, in particular when the total elastic scattering cross section given by Arndt et al. and the Nijmegen group is used to normalize the data. A Legendre polynomial fit to the existing $n-p$ scattering data in the 14 MeV energy region, excluding the present measurement, showed that a best fit is obtained for a second order expansion. Furthermore, the Kolmogorov-Smirnov test confirms the general agreement in the backward scattering hemisphere and shows that significant differences between the database and the predictions occur in the angular range between 60° and 120°, and below 20°. Although there is good overall agreement in the backward scattering hemisphere, more precision small-angle scattering data and a better definition of the total elastic cross section are needed for an accurate determination of the shape and magnitude of the angular distribution.

PACS numbers: 13.75.Cs, 24.40.Dn

## I. INTRODUCTION

The *n-p* differential scattering cross section is one of the basic tools used to study the nuclear force. Despite its importance as a primary standard in nuclear physics where it is used to determine neutron fluence and neutron cross sections, it has yet to meet the precision sometimes required by modern applications such as detector calibration, nuclear theoretical calculations and other computer modeling of physical processes where neutrons are involved. In fact, most measured data [1–8] for *n-p* scattering in the 14 MeV neutron energy range are dated and not of a precision expected for such a basic standard. The more recent measurements of Bürkle et al. [9] and Kondo et al. [10] have rather limited angular ranges thus making the normalization to the total elastic scattering cross section less accurate. In addition to large estimated uncertainties in many of the individual measurements, these data sets differ significantly and are not in good agreement with the model-based predictions nor with the evaluated data (see FIG. 1). The current version of the phase-shift analysis of Arndt et al. [11] as obtained from Ref. [12], the Nijmegen group [13, 14] and the ENDF/B-VII.0 evaluation [15], henceforth labeled "the three predictions", do not use the same experimental database, which can lead to differences beyond the formal differences in their approaches. A calculation that uses this scattering cross section as input, in this energy region, is bound to suffer from additional uncertainties in its results introduced by the lack of accuracy in the standard. Refinements and advances in theoretical modeling and data evaluation over the last three decades require a more accurate database in the 14 MeV region to test their results. We have undertaken a series of experiments to measure this scattering cross section with greater accuracy than in currently available data. A major improvement in the present measurement over most previous ones is the larger angular range covered by a set of fixed-angle $\Delta E$-$E$ telescopes. Recoil protons were detected between 0° and 60° in the laboratory system (about 180° to 60° in the center-of-mass (c.m.) system for the neutron) resulting in a better determination of the angular distribution with reduced systematic uncertainties. Further improvements came from the use of up-to-date electronics and computer systems to achieve cleaner recoil proton spectra with minimum dead time. This work is an extension of our previous measurements at 10 MeV [16] with these new techniques.

## II. EXPERIMENTAL DETAILS

### A. Experimental Details

Neutrons were produced at the Ohio University Edwards Tandem Accelerator laboratory by the $^3$H(d, n)$^4$He reaction using a continuous beam of 460 ± 5 keV deuterons directed onto a tritiated titanium target. The neutron-producing target consisted of a tritiated titanium layer, approximately 2.0 mg/cm$^2$ on a 0.5 mm silver backing. A wobbler was used to help diffuse the heating in the target which was air-cooled. With this deuteron beam energy and a stopping titanium target uniformly loaded with tritium, the mean energy of the neutrons produced at 0° is 14.9 MeV with a HWHM of approximately 0.3 MeV. These source neutrons were collimated to a spot size of approximately 1 cm diameter on a 3.8 mg/cm$^2$-thick polypropylene foil mounted on a 0.5 mm thick tantalum backing located 50.3 cm from the neutron-producing target.

The experiment consisted in counting recoil protons from *n-p* scattering in the polypropylene foil. The detector system was made of eleven fixed $\Delta E - E$ telescopes located at 0°, ±12°, ±24°, ±36°, ±48° and ±60° with respect to the neutron beam axis. The general layout of the scattering chamber and telescope system was previously described in detail in Ref. [16] with the difference that the telescope collimators used in the present experiment were 0.4 mm thick to stop the higher energy recoil protons. Detectors of adequate thicknesses were utilized to accomodate the higher recoil proton energies of the present experiment. These telescopes were housed in a well-shielded scattering chamber shown in FIG. 2, and were located symmetrically with respect to the incident neutron beam axis to minimize systematic errors in scattering angle determination, and to provide redundant independent and simultaneous measurements in addition to improving counting rates. It was then possible, with this fixed-angle detecting system, to optimize detector thicknesses for the recoil proton energy available at each angle. Furthermore, the telescope system eliminated the necessity of accurate monitoring of the neutron beam intensity which was the case in a number of previous measurements where data were taken one angle at a time.

Relative solid angle normalization was obtained by counting particles emitted by a highly uniform $^{239}$Pu $\alpha$-source. An NE213 neutron detector equipped with n-$\gamma$ discrimination capability located 90° relative to the deuteron beam was utilized to normalize the output of the neutron source for the sample-in versus sample-out runs. A further check of this normalization was provided by the (n,p) and (n,$\alpha$) reactions in the silicon of the 0° detector. There was excellent agreement between these methods (less than 0.3% difference). Background was estimated from sample-out runs that were taken in alternated fashion with the sample-in runs. The sample-out runs used a blank target consisting of a tantalum backing without the polypropylene foil.

### B. Electronics and Data Acquisition System

Signal handling techniques used in the present measurement were similar to those used in Ref. [16]. However, a major effort was made to improve the data acquisition system (DAQ) by minimizing dead time problems and noise cross-talk from a summing amplifier [17]. Each individual telescope was thus handled separately by a dedicated DAQ consisting of a data acquisition board mounted in a separate independent personal computer. An additional data acquisition board and computer were used for the NE213 neutron monitor. A distributed DAQ system was achieved by connecting the 12 individual DAQ systems to a master personal computer to synchronize data acquisition start and stop times for all telescopes and the neutron monitor. Data were taken in event mode for later replay and analysis.

## III. DATA ANALYSIS, CORRECTIONS AND UNCERTAINTIES

### A. Data reduction

The data reduction procedure used in the present work was previously described in detail in Ref. [16]. Individual experimental runs were carefully screened before inclusion in the final data used in the computation of the angular distribution. $\Delta E - E$ scatter plots (FIG. 3,4) were generated for each telescope from the corresponding event stream. Regions of interest (ROI) were drawn around recoil protons and used subsequently to gate the event stream for both sample-in and sample-out runs. Proton yields were obtained for the gated foreground and background data and normalized using the NE213 neutron monitor. The normalized gated background data were then subtracted from the sample-in data and net proton yields were obtained. FIG. 5 shows a sample of background-corrected recoil proton histograms for 3 different telescopes. The effects on the proton yields of the $\Delta E - E$ gate size and shape were also investigated in detail using ROI of different shapes and sizes. The proton groups in the $\Delta E - E$ ROI were in most cases well-defined but somewhat less so for the 0°, 48° and 60° telescopes where background levels relative to the proton events of interest were significantly higher than at other angles.

### B. Corrections

The relative solid angle normalization coefficients shown in FIG. 6 were obtained from the $^{239}$Pu $\alpha$-source and were used to normalize the net proton yields. The advantages of this normalization procedure reside in its consistency and the statistical nature of the related uncertainties. All but the 60° telescopes were fitted with similar circular solid-angle defining collimators located in front of the ΔE detectors. The 60° telescopes were

equipped with slit-shaped collimators with rounded edges mounted in the vertical plane to diminish the important kinematic spread observed at this angle at the expense of a reduced solid angle, and thus counting rate, as seen in FIG. 6. Dead time corrections were less than 0.01% due to the improvements in the DAQ system [17]. Counting losses due to multiple scattering in the target and in the ΔE detector and finite size effects, including the mean scattering angle, were estimated with a Monte Carlo calculation as described previously [16]. They were significant for the 48° and 60° angles. Relativistic kinematics was used to calculate the c.m. relative angular distribution.

### C. Uncertainties

Uncertainties indicated in Table I are the estimated overall uncertainties for the present measurement and are essentially statistical. In addition to counting uncertainties, they include the following contributions:

1. The uncertainty in the normalization of the sample-in data set to that of the sample-out (0.2-0.3%). It was estimated from the normalization factors obtained by using the NE213 monitor and the $^{28}$Si(n,p) and $^{28}$Si(n,$\alpha$) reactions in the 0° telescope.

2. The uncertainty in the determination of the solid angle normalization which was essentially statistical (0.2%). Using the $\alpha$ source and fixed-angle $\Delta E - E$ telescopes greatly reduces the systematic errors of this type encountered in single-telescope measurements.

3. The uncertainty in the gate size and shape that delimits the region of interest (0.3%). It was inferred from the relative proton yield difference for the largest and smallest $\Delta E - E$ ROI used to gate the event stream.

4. The uncertainty in the Monte Carlo counting-loss calculations due to multiple scattering and finite-size effects (0.25%). They were estimated by varying the seed of the random number generator in addition to the purely statistical uncertainty due to the number of histories used in the calculations.

These contributions were combined in quadrature to obtain the estimated overall uncertainty.

## IV. RESULTS AND DISCUSSION

### A. Results

The c.m. relative angular distribution was fitted with Legendre polynomial expansions, integrated and normalized to the ENDF/B-VII.0 evaluation total elastic scattering cross section value $\sigma_{el}^{tot} = 647.42$ mb [15] to obtain the angular distribution values listed in Table I and shown in FIG. 7. However, the total elastic scattering cross section given by the ENDF/B-VII.0 evaluation differs, surprisingly, with those of the Arndt and Nijmegen groups by nearly 1 % as shown in Table II. This is a further indication of the disagreements in the results given by the three methods. All calculations and comparisons shown below were duplicated using the total elastic scattering cross section value of 653.5 mb given by the Arndt and Nijmegen groups and the results are discussed in section IV.B.3.

The uncertainties listed in Table I are essentially statistical in nature. The background was the second most significant source of uncertainties for the forward c.m. direction (60° and 84°) and was negligible at the other angles. The c.m. angular distribution was expressed as:

$$\sigma(\theta_{cm}) = a_0 + a_1 P_1 + a_2 P_2 + a_3 P_3 + a_4 P_4 \qquad (1)$$

$P_i$ in this expansion is the Legendre polynomial of order $i$. The number of terms in this expansion was limited by the number of degrees of freedom $\nu$. Furthermore, the lack of data in the forward c.m. direction, in addition to the larger uncertainty in the 60° data point, limited the highest practical polynomial order required for a physically reasonable fit to 2. The results for a first order ($P_1$) and second order ($P_2$) Legendre expansions are listed in Table III and shown in FIG. 7. Although the $P_1$ and $P_2$ fits had similar $\chi^2$ values and hence are equally probable, there was a significant difference in shape between the two fits. While the $P_1$ fit was backward-peaked, in agreement with all of the shapes predicted by Arndt et al., the Nijmegen group and the ENDF/B-VII.0 evaluation, the $P_2$ shape was forward and backward-peaked, as illustrated in FIG. 7 and FIG. 8 , in apparent agreement with the measurement of Suhami et al. [4] which covered the forward c.m. scattering direction. The latter fit is therefore not a monotonically increasing function of the c.m. scattering angle as systematically indicated in Refs [11, 13–15, 18]. The resolution of this discrepancy requires more precision data at small c.m. scattering angles to constrain the fitting procedure in that region.

### B. Discussion

#### 1. $\chi^2$ Comparisons

The absolute angular distribution was then compared to the most recent predictions of Arndt et al. obtained from Ref. [12], those of the Nijmegen [13, 14] group, and to the ENDF/B-VII.0 evaluation [15] using Pearson's $\chi^2$ statistic defined by:

$$\chi^2 = \sum_{i=1}^{N} \left( \frac{\sigma_i^{\text{experiment}} - \sigma_i^{\text{model}}}{\Delta\sigma_i} \right)^2 \qquad (2)$$

where $\Delta\sigma_i$ is the experimental uncertainty for the $i^{th}$ data point, N is the number of data points, ${\sigma_i}^{\rm experiment}$ represents the experimental data and ${\sigma_i}^{\rm model}$ is the model-based scattering cross section value to which the data are being compared. The values of the $\chi^2$ statistic and its associated probability were computed for the present data sets obtained using the $P_1$ and $P_2$ fits, and for all three current predictions under consideration, as obtained from Refs. [12, 14, 15], and are shown in Table IV. The $\chi^2$ statistic indicated better quantitative agreement of the present $P_1$-normalized data with the Arndt and Nijmegen predictions than with the ENDF/B-VII.0 evaluation. The ENDF/B-VII.0 evaluation is however, in the case of a $P_2$-normalized data, the most probable of the predictions (see Table IV). The magnitude of the forward-backward anisotropy in the final angular distribution expressed by the ratios $\frac{\sigma(180^\circ)}{\sigma(0^\circ)}$ and $\frac{\sigma(180^\circ)}{\sigma(90^\circ)}$ are listed in Table V and showed a general agreement in the backward direction of both fits with all three predictions, but indicated a significantly higher anisotropy of the $P_1$ fit in the forward direction than what is given by $P_2$ and the three predictions. In conclusion, the $P_1$ fit to the present data compares with higher probabilities to all the Arndt and Nijmegen predictions while the ENDF/B-VII.0 evaluation is the most probable of the three predictions in the case of a $P_2$ fit to the present data bearing in mind that the present data were normalized to the total elastic scattering cross section given by ENDF/B-VII.0 . These results should be compared to the results of a renormalization of the present data to the total elastic scattering cross sections of Arndt and Nijmegen as described in section IV.B.3 .

Furthermore, previous experimental data near 14 MeV [1–10], excluding the present data, were converted to our 14.9 MeV scattering energy using a linear interpolation of the total elastic scattering cross section of Ref. [15] and consolidated into a single $n-p$ scattering database, henceforth referred to as the "$n-p$ scattering database". This procedure assumes that only the magnitude and not the shape of the angular distribution is altered for the small energy shifts under consideration. This is certainly true for all those data sets which have large uncertainties attached to them. The energy differences between our bombarding energy and those of past measurements are small enough to justify this conversion.

This database was fitted with a Legendre polynomial expansion of various orders. FIG. 9 shows that the most probable fit in this case is obtained for a second order expansion and that higher order expansions do not improve the fit. The parameters of this most probable fit are listed in Table III and illustrated in FIG. 10 which compares this fit to the present data and to the three predictions. The $P_2$ fit to the present data is similar to the fit representing the $n-p$ scattering database. The two curves have the same curvature and intersect near 95°, although the scattering database shows a slightly higher (about 4%) forward-backward c.m. anisotropy than what is obtained for a $P_2$ fit to the present data as indicated in Table V. This is an additional element in favor of a $P_2$ shape for the scattering cross section in the 14 MeV energy region. There is but a single small-angle $n-p$ angular distribution measurement, namely that of Suhami et al. [4]; Additional measurements in this scattering region would significantly improve the overall definition of the $n-p$ scattering database near 14 MeV.

### 2. *The Kolmogorov-Smirnov Test*

The Kolmogorov-Smirnov test (KS) is a simple form of minimum distance estimation of goodness-of-fit used routinely in statistics to compare a sample to a given distribution represented by the cumulative distribution function (CDF) $F(x)$ under the independent-and-identically-distributed-random-variable assumption. This is the so-called one-sample KS test. It can also be used to compare two statistical samples without any assumption regarding the nature of their parent distributions and is known in that case as the two-sample KS test. The statistical sample is represented by a cumulative empirical distribution function $S_N$ which assigns a probability $1/N$ for each observation $i$ in a sample of N ordered data points of a single random variable $X$, and it is given by the step function:

$$S_N(x) = \frac{number\,of\,elements\,in\,the\,sample \leq x}{N} \qquad (3)$$

This is based on the fact that the CDF is uniformly distributed and therefore each observation contributes equally to the CDF. There are many implementations of the KS statistic $D$. In the one-sample case, it is defined as in Refs. [19–22]:

$$D = \sup |S_N(x) - F(x)| \qquad (4)$$

The probability that a KS statistic will exceed a value $u$ for the null hypothesis in the one-sample case is

$$P(u) = 2\sum_j (-1)^{j-1} e^{-2j^2u^2}$$

where $u = D\sqrt{N}$. The KS test was implemented in the present context to compare the three predictions and the fits to the present data to the existing $n-p$ scattering database by defining the KS statistic D as follows:

$$D = \sup_{0\leq\theta\leq\pi} |S_N(\theta) - F(\theta)| \qquad (5)$$

and

$$S_N(\theta) = \frac{1}{2\sigma_{el}^{tot}} \int_0^\theta \sigma(\theta')\, d\cos(\theta') \qquad (6)$$

where $S_N(\theta)$ is the empirical cumulative distribution function for the existing $n-p$ scattering database. The angle $\theta$ is the c.m. scattering angle and replaces $x$; $N$ is

the number of data points in the database and $F(\theta)$ is defined similarly to $S_N(\theta)$ but for one of the three predictions or one of the fits to the present data. $S_N(\theta)$ represents the probability of scattering a neutron at angles smaller than $\theta$ and is a measure of the shape of the angular distribution $\sigma(\theta)$. These partial cumulative scattering cross sections were calculated by simple trapezoidal integration for the $n-p$ scattering database, the three predictions, the two fits to the present data and the corresponding six data points. They are shown in FIG. 11 which provides further illustration of the good agreement among the empirical CDF's of the present six data points and their two fits, the predictions of the Arndt and Nijmegen groups and the ENDF/B-VII.0 evaluation.

The statistic D defined by equation (5) is a measure of the shape difference between an empirical cumulative distribution function $S_N(\theta)$ of N ordered data points representive of the $n-p$ scattering database and $F(\theta)$ which stands for the CDF of one of the predictions or the fits to the present data. The values of $D$ and their associated probabilities were calculated (see Table VI) and showed, as they should, no significant differences among the three predictions, the $P_1$ and $P_2$ fitted values, and the existing experimental database. Although the statistic $D$ does not differentiate the three predictions and the two fits to the present data (see FIG. 11), the quantity $D_\theta = |S_N(\theta) - F(\theta)|$ is a good measure of the local differences between the $n-p$ database and the reference CDF $F(\theta)$ as illustrated in FIG. 12. It provides a deeper insight into the structure of the $n-p$ scattering database. The largest local differences are observed between 60° and 80°, and below 20°, with smaller differences occuring above 120° and in the 40° scattering region. Large differences are an indication of the scattering regions where the techniques used to measure the $n-p$ scattering database are the least precise. The associated particle method was used to measure the scattering data in the forward c.m. hemisphere [4] and is the least precise below 20° due to the low energy of the recoil protons and the large background levels in the target detector. The small values of $D_\theta$ occur near 40° and correspond to scattering angles where this method is most precise.

On the other hand the telescope method is the prevalent technique used for measurements in the backward c.m. hemisphere where either neutrons or protons are counted. The largest $D_\theta$ values occur below 120° c.m. scattering angles, where this method is the least precise because of the low energy recoil particles available for detection by the telescope and the higher background levels, relative to the proton events of interest, induced by the reduction in the $n-p$ scattering cross section. For c.m. scattering angles larger than 120°, the telescope method can be quite accurate and overall uncertainties in the 1% range can be achieved [16].

### 3. Alternative Normalization of the Data

Because of the discrepancy in the total elastic scattering cross section given by the three predictions, a second normalization of the data was carried out using the value given by Ref. [13, 14, 23] $\sigma_{el}^{tot} = 653.5$ mb. The calculations and comparisons described above were similarly applied to the renormalized data. The shape of the angular distribution is not altered by the renormalization. The results of a $\chi^2$ comparison similar to that of section IV.B.1 are listed in Table VII and show that the Arndt and Nijmegen predictions provide a better description of the renormalized $P_1$-fitted present data than the ENDF/B-VII.0 evaluation, while the ENDF/B-VII.0 evaluation was the best description of the renormalized $P_2$-fitted data. An accurate determination of the shape and normalization of the $n-p$ angular distribution from measurements of that distribution is therefore dependent on a precise knowledge of the total elastic scattering cross section in this energy region.

### 4. Comparison of the Two Normalizations

We define the figure of merit

$$F = 100 \times \left(1 - \frac{|P_{\chi^2}(\nu) - 0.5|}{0.5}\right) \tag{7}$$

where

$$P_{\chi^2}(\nu) = \int_{\chi^2}^{\infty} P_{\chi^2}\left(x^2, \nu\right)\, dx^2$$

is the $\chi^2$ associated probability and represents the probability of observing a higher $\chi^2$ value in a random sampling of the parent distribution. $P_{\chi^2}\left(x^2, \nu\right)$ is the $\chi^2$ probability density as defined in Ref. [24]:

$$P_{\chi^2}\left(x^2, \nu\right) = \frac{\left(x^2\right)^{\frac{\nu-2}{2}} e^{\frac{-x^2}{2}}}{2^{\frac{\nu}{2}}\Gamma\left(\frac{\nu}{2}\right)}$$

Equation (7) compares a given $\chi^2$ associated probability with that of the most probable distribution, namely $P_{\chi^2}(\nu) = 0.5$, that would yield the best fit with $\chi^2_\nu = 1$. $F$ ranges from 0 to 100 and provides a quantitative measure of the agreement between the data and the predictions. The calculated values of $F$ obtained using the total elastic cross sections given by the ENDF/B-VII.0 evaluation (A) and the Arndt-Nijmegen predictions (B) are listed in Table VIII which shows that the best description of our data was obtained for the ENDF/B-VII.0 evaluation when the present data are normalized to (B) using a $P_2$ fit, while if (A) and a $P_1$ Legendre polynomial expansion were used for normalization, the second best description of the data was obtained for the Arndt et al. prediction.

## V. CONCLUSIONS

The H(n,n)H angular distribution was measured at 14.9 MeV neutron energy with high statistical precision and with a larger angular range than in most previous measurements. The $P_1$-normalized data were generally in good agreement with the Arndt et al. partial wave analyses and the Nijmegen potential, but less so with the ENDF/B-VII.0 evaluation, although the anisotropy in this case is not reflected by any of the predictions. The $P_2$-normalized data were closer to the ENDF/B-VII.0 evaluation than to the other predictions. The most probable Legendre polynomial fit to the existing $n-p$ scattering database in the 14 MeV energy region is a second order expansion and is similar to the second order fit to the present data. The present data suggest the possible existence of a local peak at 0°, which does not appear in any of the three predictions. The only small-angle scattering data available in the 14 MeV energy region, namely that of Suhami and Fox [4] seen in FIG. 1, hint at the existence of this forward peak. The best description of the present data was obtained for the ENDF/B-VII.0 evaluation when a second order Legendre polynomial fit to the present data and the Arndt et al. and the Nijmegen total elastic cross section value were used. Despite the good agreement in the backward scattering hemisphere between the present data, the second order fit to the $n-p$ scattering database and the three predictions, the shape and magnitude of the angular distribution in the forward c.m. direction remain an open question. Further small-angle precision data are required to effectively constrain the fitting procedures. A more precise determination of the total elastic scattering cross section is also needed.

## ACKNOWLEDGMENTS

The authors wish to thank John E. O'Donnell for his help with accelerator operations and Devon Jacobs for maintaining the accelerator. Additional thanks to David Gilliam of NIST for providing the $^{239}$Pu $\alpha$-source and to Arjan Plompen of IRMM for the loan of the tritium target.

[1] J. Allred, A. Armstrong, and L. Rosen, Phys. Rev. **91**, 90 (1953)
[2] J. D. Seagrave, Phys. Rev. **97**, 757 (1954)
[3] T. Nakamura, Phys. Soc. Japan **15**, 1359 (1960)
[4] A. Suhami and R. Fox, Phys. Lett. **24B**, 173 (1967)
[5] E. Greiner and H. Karge, Ann. Phys. **16**, 354 (1967)
[6] I. Basar, in *Light Nuclei and Nuclear Interactions*, Few Body Problems, Vol. 2, edited by G. Paić and I. Ŝlaus (Gordon and Breach Science Publishers, New York, 1968) p. 867, proceedings of the symposium held in Brela, Yugoslavia, 1967
[7] M. Tanaka, N. Koori, and S. Shirato, J. Phys. Soc. Japan **28**, 11 (1970)
[8] S. Shirato and K. Saitoh, J. Phys. Soc. Japan **36**, 331 (1974)
[9] W. Bürkle and G. Mertens, Few-Body Systems **22**, 11 (1997)
[10] K. Kondo, I. Murata, K. Ochiai, *et al.*, Nucl. Inst. Meth. **A 568**, 723 (2006)
[11] R. A. Arndt, W. J. Briscoe, I. I. Strakovsky, and R. L. Workman, Phys. Rev. **C 76**, 025209 (2007)
[12] "*SAID* partial-wave analysis facility," `http://gwdac.phys.gwu.edu/analysis/nn_analysis.html`
[13] J. J. de Swart *et al.*, Few-Body Systems **Suppl. 8**, 438 (1995)
[14] "Theoretical high energy physics group of the radboud nijmegen university," `http://nn-online.org/NN/`
[15] A. D. Carlson *et al.*, Nuclear Data Sheets **110**, 3215 (2009)
[16] N. Boukharouba, F. B. Bateman, C. E. Brient, A. D. Carlson, S. M. Grimes, R. C. Haight, T. N. Massey, and O. A. Wasson, Phys. Rev **C 65**, 014004 (2002)
[17] F. B. Bateman, S. I. Al-Quraishi, C. E. Brient, N. Boukharouba, A. D. Carlson, S. M. Grimes, R. C. Haight, T. N. Massey, and R. T. Wheeler, in *International Conference on Nuclear Data for Science and Technology*, AIP Conference Proceedings, Vol. 769, edited by R. C. Haight, M. B. Chadwick, T. Kawano, and P. Talou (Melville, NY, ISBN 0-7354-0254-X, 2005) p. 656, conference held in Santa Fe, New Mexico, USA, September 26-October 1, 2004
[18] R. A. Arndt, I. I. Strakovsky, and R. L. Workman, Phys. Rev. **C 50**, 2731 (1994)
[19] W. H. Press *et al.*, *Numerical Recipes in Fortran 77: The Art of Scientific Computing*, 2nd ed. (Cambridge University Press, ISBN 052143064-X, 2003)
[20] A. Stuart, K. Ord, and S. Arnold, *Kendall's Advanced Theory of Statistics*, 6th ed., Vol. 2A: Classical Inference and the Linear Model (Wiley & Sons, ISBN-10: 0340662301, 2009) pp. 25.37–25.43
[21] W. T. Eadie, D. Drijard, F. James, M. Roos, and B. Sadoulet, *Statistical Methods in Experimental Physics* (North-Holland, Amsterdam, 1971) p. 269271
[22] I. M. Chakravarti, R. G. Laha, and J. Roy, *Handbook of Methods of Applied Statistics*, Vol. 1 (John Wiley and Sons, 1967) pp. 392–394
[23] R. A. Arndt, W. J. Briscoe, A. B. Laptev, I. I. Strakovsky, and R. L. Workman, Nucl. Sci. & Engineering **162**, 312 (2009), `http://gwdac.phys.gwu.edu/analysis/nn_analysis.html`
[24] P. R. Bevington and D. K. Robinson, *Data Reduction and Error Analysis for the Physical Sciences*, 3rd ed. (McGraw-Hill, ISBN 0-07-247227-8, 2003)

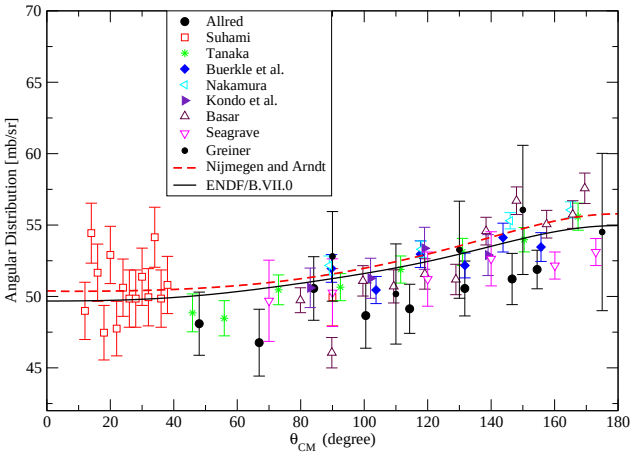


FIG. 1. (color online) Comparison of existing data from past measurements with the ENDF/B-VII.0 evaluation, the Arndt et al. and Nijmegen predictions. All data were scaled to a 14.9 MeV bombarding energy using a linear interpolation of the ENDF/B-VII.0 evaluation of the total elastic cross section [15].

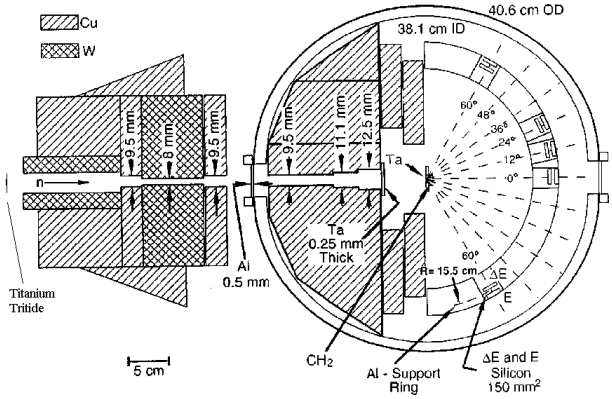


FIG. 2. Layout of the scattering chamber, neutron source, telescope system and shielding.

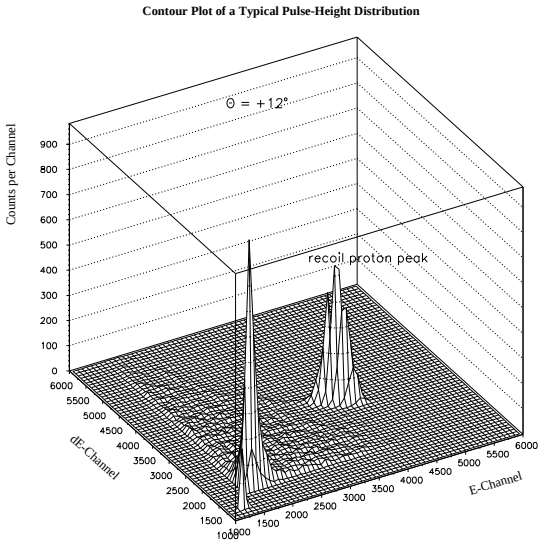


FIG. 3. A sample $\Delta E - E$ three-dimensional plot of the telescope located at $\theta = 12°$. The recoil proton group of interest appears near the center of the plot.

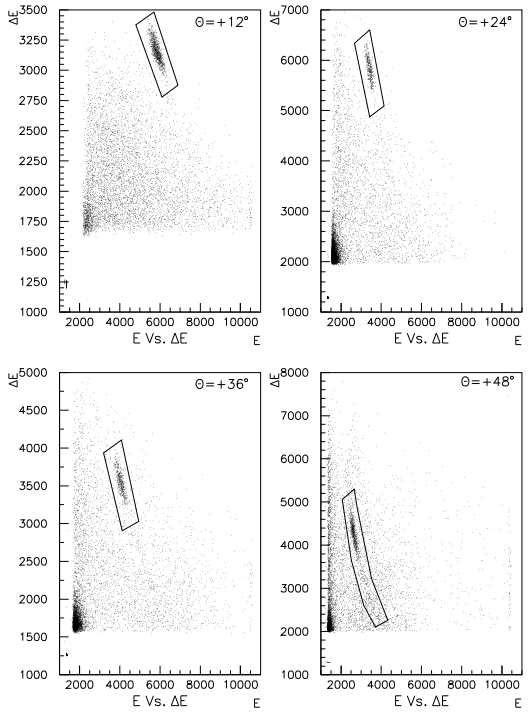


FIG. 4. Typical $\Delta E - E$ recoil proton scatter plots with the regions of interest used to gate the event stream. The numbers on the horizontal and vertical axes are the channel numbers.

Summary of Experimental Data

| $\theta_{cm}$ (°) | $\sigma(\theta_{cm}) \pm \Delta\sigma$ (mb/sr) | $\sigma(\theta_{cm}) \pm \Delta\sigma$ (mb/sr) | Uncertainty (%) |
|---|---|---|---|
| | $P_1$ fit | $P_2$ fit | |
| 175.3 | 55.23 ± 0.85 | 54.37 ± 0.82 | 1.54 |
| 155.5 | 55.11 ± 0.51 | 54.26 ± 0.49 | 0.92 |
| 131.7 | 53.10 ± 0.61 | 52.27 ± 0.59 | 1.14 |
| 107.7 | 52.66 ± 0.65 | 51.84 ± 0.63 | 1.24 |
| 83.8 | 51.51 ± 0.92 | 50.71 ± 0.89 | 1.79 |
| 59.7 | 49.80 ± 3.60 | 49.02 ± 3.50 | 7.18 |

TABLE I. Values of the measured angular distribution obtained from a normalization of the angle-integrated experimental scattering cross section to the ENDF/B-VII.0 evaluation [15] total elastic cross section. $\theta_{cm}$ is the mean c.m. neutron scattering angle (in degrees) calculated by Monte Carlo integration.

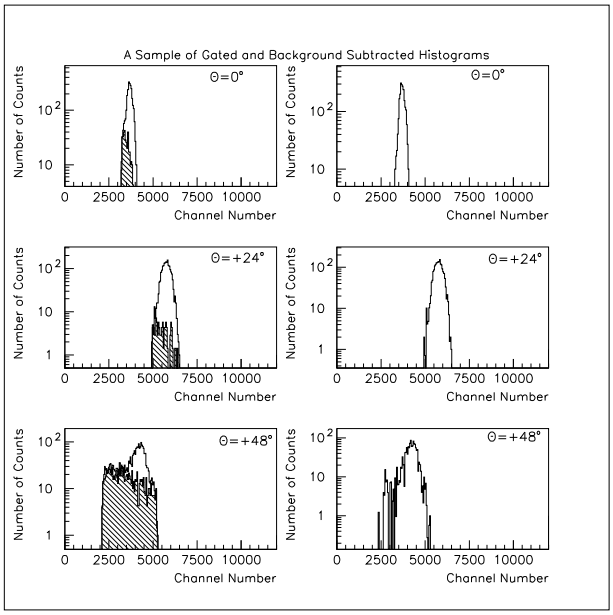


FIG. 5. Typical gated and background-corrected histograms. The graphs on the left-hand-side show an overlay of the background and the foreground on a log scale. The normalized background is shown in hatched style. The right-hand-side column shows the net background-corrected recoil proton peak.

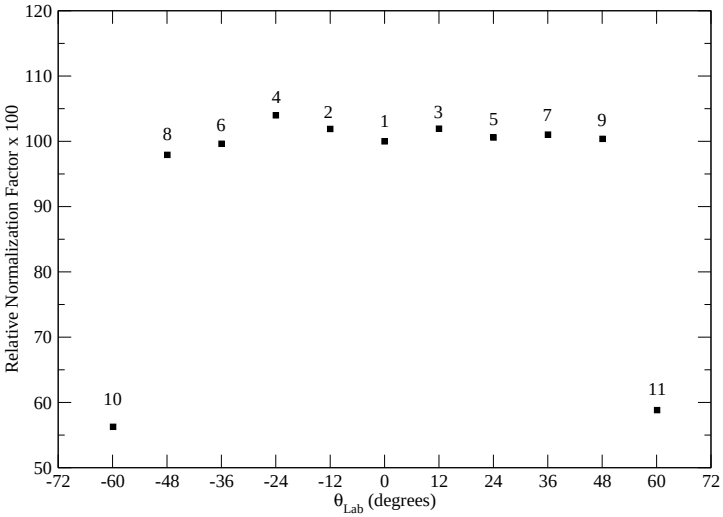


FIG. 6. Relative solid angle normalization factors (in %) obtained from the $^{239}$Pu $\alpha$ source for the August-September 2007 experiment run. The $\alpha$ -particle yields were normalized to the telescope located at $\theta = +12^{\circ}$. The numerical labels attached to the data points represented by squares indicate the telescope number. Beam left telescopes are even numbered

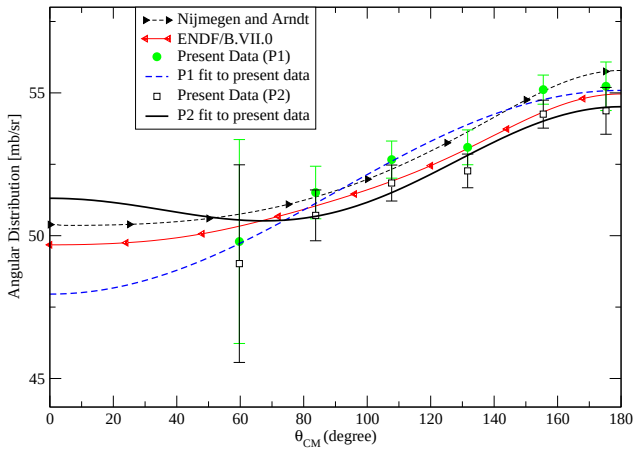


FIG. 7. (color online) H(n,n)H differential scattering cross section at a neutron energy of 14.9 MeV compared to the predictions of Nijmegen, Arndt et al. and to the ENDF/B-VII.0 evaluation. The $P_1$ and $P_2$ fits are fits to the experimental data that require that the integrated angular distribution for each be 647.42 mb. Since the angular distributions are not exactly the same for the P1 and P2 fits, the normalizations of the data points differ for the two fits.

Neutron Total Elastic scattering cross sections

| | $\sigma_{tot}^{el}$ (mb) |
|---|---|
| ENDF/B.VII.0 [15] | 647.4 |
| Nijmegen [13, 14] | 653.5 |
| Arndt et al. [12] | 653.5 |

TABLE II. Total elastic cross sections for scattering 14.9 MeV neutrons on hydrogen.

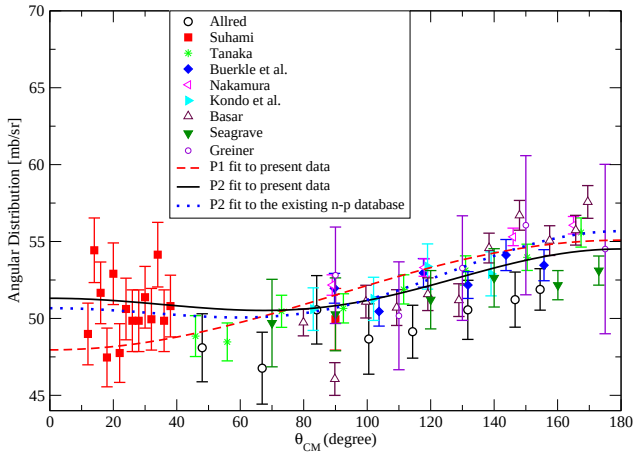


FIG. 8. (color online) Comparison of a $P_2$ fit to the existing $n-p$ elastic scattering database, described in section IV.B.1, with the $P_1$ and $P_2$ fits to the present data.

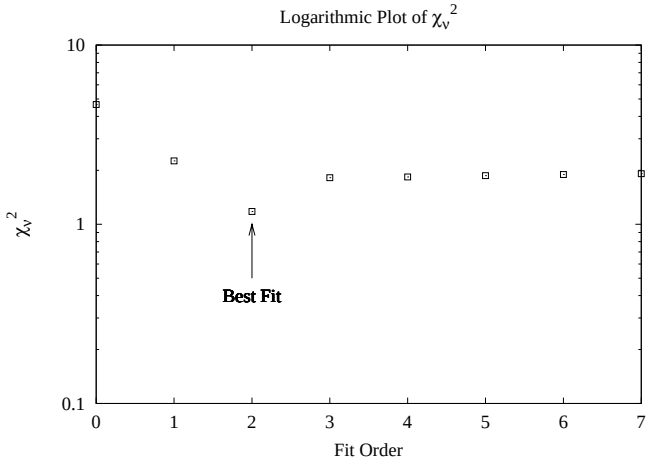


FIG. 9. Logarithmic plot of $\chi^2_\nu$, the reduced Pearson statistic, as a function of the order of the Legendre polynomial expansion used to fit the $n-p$ scattering database in the 14 MeV region. The data were converted to $E_n = 14.9$ MeV using a linear interpolation of the ENDF/B-VII.0 total elastic scattering cross section as described in section IV.B.1.

Least-square Fit Parameters

| | $P_1$ Fit | $P_2$ Fit | $n$-$p$ Data Base |
|---|---|---|---|
| $a_0$ (mb/sr) | 51.52 | 51.52 | 51.52 |
| $a_1$ (mb/sr) | $-3.55 \pm 0.28$ | $-1.60 \pm 0.44$ | $-2.51 \pm 0.29$ |
| $a_2$ (mb/sr) | | $1.40 \pm 0.53$ | $1.65 \pm 0.30$ |
| $\chi^2_\nu$ | 0.49 | 0.40 | 1.18 |
| $\chi^2$- probability (%) | 69 | 67 | 16.3 |

TABLE III. Parameters of the Legendre polynomial fits. This table lists the parameters of the first order ($P_1$) and second order ($P_2$) fits to the present data and the most probable fit (*i.e.* $P_2$) to the $n-p$ scattering data base described in section IV.B.1. The parameter $a_0$ does not have an uncertainty because it was normalized to the total elastic cross section given by the ENDF/B-VII.0 evaluation.

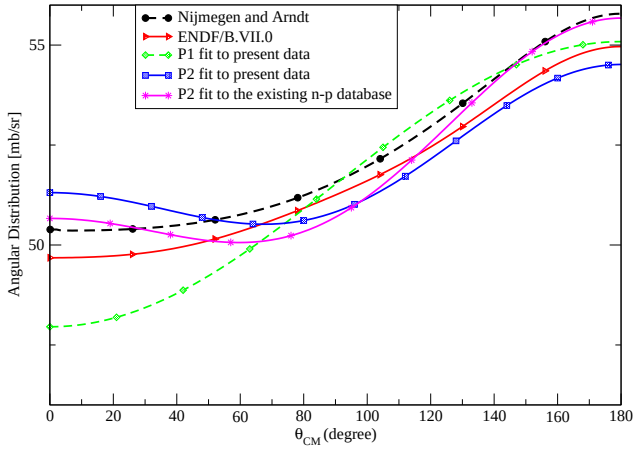


FIG. 10. (color online) Comparison of the most probable fit to the existing $n-p$ elastic scattering database, described in section IV.B.1, with the $P_1$ and $P_2$ fits to the present data, the predictions of the Arndt and Nijmegen groups, and the ENDF/B-VII.0 evaluation. The $P_2$ fit to the present data is the most suitable representation of the shape of the $n-p$ angular distribution near 14.9 MeV.

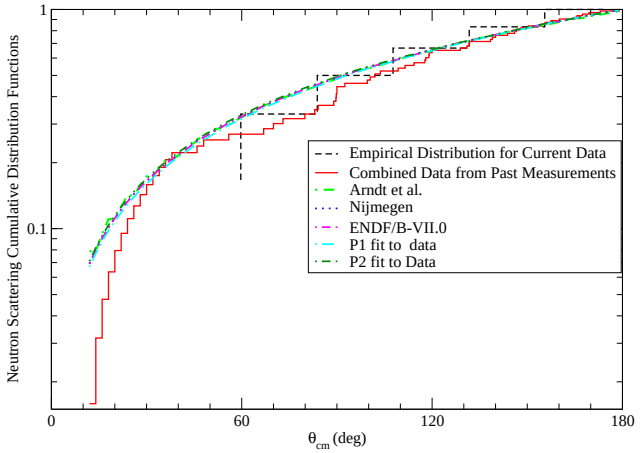


FIG. 11. (color online) Logarithmic plot of the neutron scattering cumulative distribution functions (CDF) $S_N(\theta)$ and $F(\theta)$ of equation (6). $S_N(\theta)$ is the CDF of the existing $n-p$ scattering database described in section IV.B.1 and $F(\theta)$ is the CDF of the reference distribution, namely one of the three predictions or the $P_1$ and $P_2$ fits to the present data. The CDF's for the predictions and the fits to the present data are similar and cannot be distinguished on this plot. The empirical cumulative distribution function for the present six data points are represent by the dashed line and show excellent agreement with the three predictions and the fits to the present data. There are however significant differences between the CDF's of the $n-p$ scattering database and those of the predictions and fits to the present data between $60^\circ$ and $120^\circ$ and for small c.m. angles.

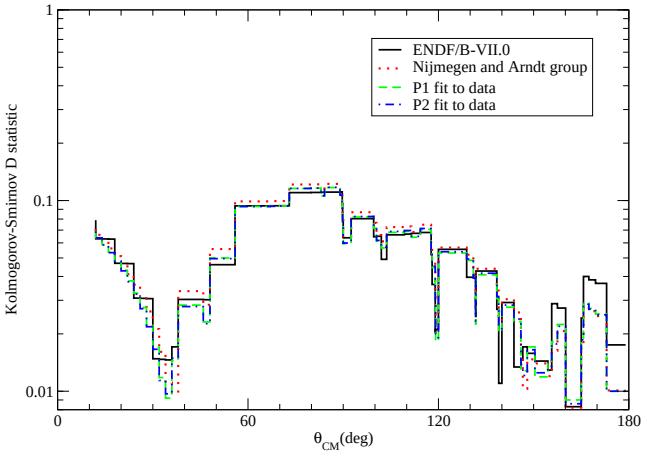


FIG. 12. (color online) Logarithmic plot of the statistic $D_\theta$ defined in section IV.B.2 and calculated for the predictions of the ENDF/B-VII.0 evaluation, the Arndt and Nijmegen groups, and the $P_1$ and $P_2$ fits to the present data. Scattering regions of minimal differences between the existing $n-p$ scattering database and the predictions are exhibited by the D-statistic.

| | $P_1$ Data | | $P_2$ Data | |
|---|---|---|---|---|
| Model | $\chi^2$ | Probability(%) | $\chi^2$ | Probability(%) |
| Arndt et al. | 1.81 | 61.3 | 12.03 | 0.2 |
| Nijmegen | 1.52 | 67.8 | 11.68 | 0.3 |
| ENDF/B-VII.0 | 4.52 | 21.1 | 2.47 | 29.1 |

TABLE IV. Summary of a $\chi^2$ comparison of the present data to the predictions of Arndt et al., Nijmegen, and the ENDF/B-VII.0 evaluation. "$P_1$ data" and "$P_2$ data" are respectively the present data sets obtained by normalization to the ENDF/B-VII.0 total elastic cross section using the first and second order Legendre polynomial fits to the present data. The individual data points are bound to differ in the two cases.

Anisotropy of the Angular Distribution

| | $\sigma(180°)/\sigma(0°)$ | | $\sigma(180°)/\sigma(90°)$ | |
|---|---|---|---|---|
| | $P_1$ | $P_2$ | $P_1$ | $P_2$ |
| Present data | 1.15 | 1.06 | 1.07 | 1.07 |
| Arndt et al. | 1.09 | | 1.09 | |
| Nijmegen | 1.08 | | 1.08 | |
| ENDF/B-VII.0 | 1.07 | | 1.07 | |
| $n-p$ database | 1.10 | | 1.10 | |

TABLE V. Magnitude of the anisotropy in the angular distributions obtained from the present data and those of Arndt et al., Nijmegen, the ENDF/B-VII.0 evaluation, and the $P_2$ fit to the $n-p$ scattering database, which does not include the present data. $P_1$ and $P_2$ are the fits to the present data.

| | $D$ | Probability (%) |
|---|---|---|
| Arndt et al. [12] | 0.01743 | 95 |
| Nijmegen [13, 14] | 0.01947 | 94 |
| ENDF/B.VII.0 [15] | 0.02017 | 94 |
| $P_1$ | 0.0264 | 90 |
| $P_2$ | 0.01517 | 96 |

TABLE VI. Values of the Kolmogorov-Smirnoff statistic $D$ and its associated probability obtained from a comparison of the $n$-$p$ scattering database and the predictions of the Arndt and Nijmegen groups, the ENDF/B-VII.0 evaluation and the $P_1$ and $P_2$ fits to the present data.

| | $P_1$ Data | | $P_2$ Data | |
|---|---|---|---|---|
| Model | $\chi^2$ | Probability(%) | $\chi^2$ | Probability(%) |
| Arndt, et al. | 3.7 | 29.6 | 3.9 | 14.2 |
| Nijmegen | 3.5 | 32.1 | 3.6 | 16.5 |
| ENDF/B-VII.0 | 12.9 | 0.5 | 1.5 | 47.2 |

TABLE VII. Summary of a $\chi^2$ comparison of the present data to the predictions of Arndt et al., Nijmegen, and the ENDF/B-VII.0 evaluation. "$P_1$ data" and "$P_2$ data" are respectively the present data sets obtained by normalization to the Arndt and Nijmegen total elastic cross section using the first and second order Legendre polynomial fits to the present data.

| | $P_1$ Data | | $P_2$ Data | |
|---|---|---|---|---|
| Model | $\chi^2$ | $F$(%) | $\chi^2$ | $F$(%) |
| Arndt, et al.$^A$ | 1.8 | 77.4 | 12.0 | 0.4 |
| Nijmegen$^A$ | 1.5 | 64.4 | 11.7 | 0.6 |
| ENDF/B-VII.0$^A$ | 4.5 | 42.0 | 2.5 | 58.2 |
| Arndt et al.$^B$ | 3.7 | 59.2 | 3.9 | 28.4 |
| Nijmegen$^B$ | 3.5 | 64.2 | 3.6 | 33.0 |
| ENDF/B-VII.0$^B$ | 12.9 | 1.0 | 1.5 | 94.4 |

TABLE VIII. Summary of the figure of merit $F$ which measure the goodness-of-fit of the present data to the predictions of Arndt et al., Nijmegen and the ENDF/B-VII.0 evaluation for the two normalizations used in section IV. The superscripts correspond respectively to the cases where the ENDF/B-VII.0 evaluation ($A$) and the Nijmegen-Arndt ($B$) total elastic cross section values were used to normalize the present data. "$P_1$ data" and "$P_2$ data" are respectively the data sets obtained by normalization to the total elastic cross section using the first and second order Legendre polynomial fits to the present data.